EurJIC
European Journal of Inorganic Chemistry

Research Article
doi.org/10.1002/ejic.202300423

Chemistry Europe
European Chemical Societies Publishing

www.eurjic.org

Structural Diversity in Cyclometalated Diiridium(III) Complexes with Bridging *syn* and *anti* μ_2-Oxamidato and μ_2-Dithioxamidato Ligands

Ahmed M'hamedi,[a, b] Andrei S. Batsanov,[c] Mark A. Fox,[c] Juan A. Aguilar,[c] and Martin R. Bryce*[c]

Six new diiridium complexes containing 2-methyl-6-phenylpyridyl as the cyclometalating ligand with a μ_2-oxamidato or a μ_2-dithioxamidato ligand as the bridge have been synthesized in 60–73% yields. These complexes were revealed by multinuclear NMR spectroscopy to contain inseparable mixtures of diastereomers (*rac*, ΔΔ/ΛΛ and *meso*, ΔΛ) with bridges in *anti* and *syn* configurations. The remarkable variety of isomers present was confirmed by X-ray crystallography on single crystals grown from mixtures of each complex. In one complex with a *N,N'*-bis(4-trifluoromethylphenyl)-μ_2-oxamidato bridge, two single crystals of *anti* and *syn* isomers were structurally determined. Two single crystals of the μ_2-dithioxamidato bridge complex were found to contain *rac* and *meso* forms of the *syn* isomer. Hybrid DFT computations on the four isomers of each diiridium complex revealed negligible energetic preferences for one isomer despite the methyl groups in the 2-methyl-6-phenylpyridyl cyclometalating ligands being close to the neighboring methyl groups and the bridge, thus supporting the experimental findings of isomer mixtures. Two distinct broad emissions with maxima at 522–529 nm and at 689–701 nm observed in these complexes in dichloromethane are attributed to mixed metal-ligand to ligand charge transfer (MLLCT) excited states involving the pyridyl and bridge moieties respectively with the aid of electronic structure computations.

Introduction

Cyclometalated Ir(III) complexes continue to attract great attention due to their facile chemical modifications, readily tunable photophysical and structural properties, and their high stability.[1–10] In contrast to the extensive development of monoiridium complexes that followed the initial work by Watts and co-workers in the 1980s,[11] diiridium complexes have been largely neglected, although the bridging ligand can impart additional interesting structural and electronic variations compared to monoiridium systems.[12,13] Diiridium complexes are often obtained as a mixture of diastereomers, which are generally not separated. Representative recent examples of organic bridging ligands in diiridium complexes include derivatives of 4,6-diarylpyrimidine,[14] 2-phenylpyrimidine,[15,16] diarylhydrazide,[17,18] pyrazolate,[19,20] bis(phenanthroline)[21] Schiff bases,[22–24] pyridazine,[25] butadiene[26] and alkynes.[27]

Sünkel *et al* first reported a diiridium complex bridged by a μ_2-oxamidato-*N,N',O,O'* ligand,[28] namely complex **1** and we characterized its analogs **2a**,[29] **2b**[29] and **2c**[30] (Figure 1). As evident from NMR spectra, these complexes form as mixtures of diastereomers: enantiomers with the same (ΔΔ or ΛΛ) configurations of the two octahedral Ir centres, and the *meso* (ΔΛ) form, whereas X-ray structures revealed *meso* configurations for **1**, **2b** and **2c** (molecular symmetry C_i) but a racemic ΔΔ/ΛΛ crystal for **2a** (molecular symmetry C_2). It is noteworthy that in similar complexes with shorter bridges (e.g., μ_2-Cl) the latter option is sterically forbidden.[17,18] Another ambiguity is whether the bridging ligand has *syn*- or *anti*-configuration in these oxamidato diiridium systems. Unsubstituted oxamidato ligands in **1** and **2a** are disordered, with O and NH statistically mixed, thus X-ray evidence in favour of the *anti*-configuration is inconclusive. However, in **2b** and **2c** – the only reported derivatives to date with substituents at the bridge N atoms – the *anti*-geometry with N,O chelation at each iridium centre was proved unambiguously.[29,30]

It was, therefore, of interest to examine different cyclometalating and bridging ligands of these μ_2-oxamidato-bridged diiridium systems to see if one isomer could be isolated pure or a *syn*-isomer could be identified conclusively for the first time.[31] Here we report new complexes **3a–d**, **4** and **5** (Figure 1), containing 2-methyl-6-phenylpyridyl (2-Meppy) as the cyclometalating ligand and various oxamidato ligands or a

[a] Dr. A. M'hamedi
Department of Chemistry, College of Sciences and Humanities in Al-Kharj
Prince Sattam bin Abdulaziz University
Al Kharj 11942 (Saudi Arabia)

[b] Dr. A. M'hamedi
Department of Chemistry
University of Abdelhamid Ibn Badis BP 227
Mostaganem 27000 (Algeria)

[c] Dr. A. S. Batsanov, Dr. M. A. Fox, Dr. J. A. Aguilar, Prof. M. R. Bryce
Department of Chemistry
Durham University
South Road, Durham, DH1 3LE (United Kingdom)
E-mail: m.r.bryce@durham.ac.uk
Homepage: http://www.durham.ac.uk/staff/m-r-bryce/

Supporting information for this article is available on the WWW under https://doi.org/10.1002/ejic.202300423

Research Article
doi.org/10.1002/ejic.202300423

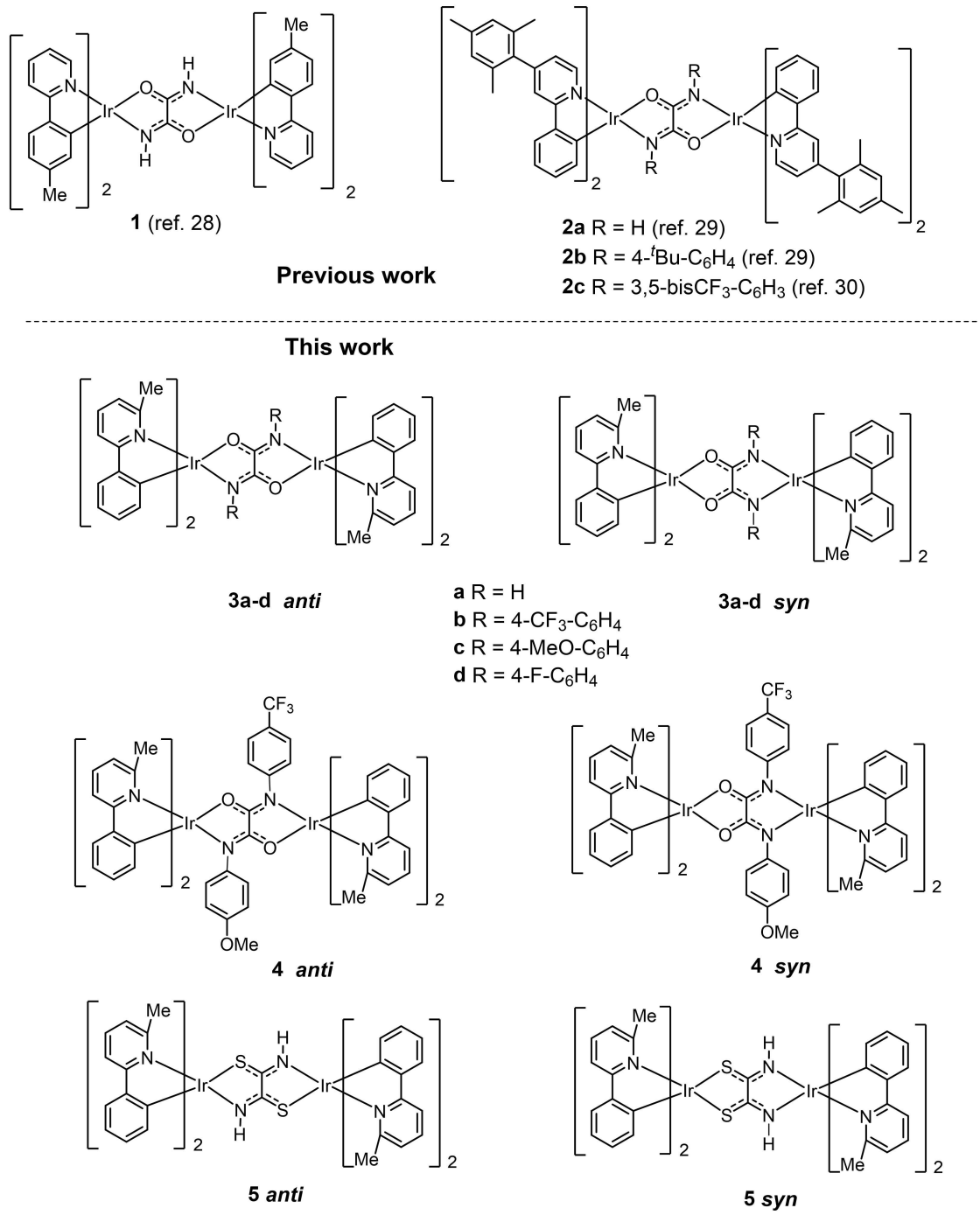

Figure 1. Structures of the μ_2-oxamidato-*N,N′,O,O′* bridged diiridium complexes **1** and **2a**–**c** reported previously, and the new complexes **3a**–**d**, **4** and **5**, synthesized in this study.

μ_2-dithioxamidato ligand [*syn* S_2C–CN_2] and/or [*anti* SNC–CNS] as the bridge. To our knowledge, the cyclometalating ligand has not been used previously in any diiridium complexes. We chose this new ligand to explore whether steric effects of the methyl group in proximity to the bridge would reduce the number of isomers synthesized, or whether the mixture of isomers produced could be successfully separated into isolated isomers. While diiridium complexes with μ_2-dithioxamidato ligand [*anti* S_2C–CN_2] or [*syn* S_2C–CN_2] as the bridge have not been reported, the structures of diruthenium and dipalladium complexes with a substituted μ_2-dithioxamidato [*anti* SNC–CNS] bridge have been determined elsewhere.[32,33] Although the isomers formed could not be isolated pure, we show the remarkable structural diversity of the *syn* and *anti* isomers from X-ray crystallography on crystals grown from isomeric mixtures containing complexes **3a**–**d**, **4** and **5**. The *syn* isomers of μ_2-oxamidato-bridged diiridium systems are reported here for the first time.

Research Article
doi.org/10.1002/ejic.202300423

Results and Discussion

Synthesis and characterization

The synthesis of the complexes was based on the procedures used for complexes **1**,[28] **2a–c**.[29,30] The μ_2-dichloro-bridged precursor [tetrakis(2-methyl-6-phenylpyridine-C^2,N')-bis(μ-chloro)diiridium(III)] was reacted with oxamide or with the appropriate *N,N'*-diaryloxalamide derivative in the presence of sodium methoxide to give **3a–d** and **4**, typically in 60–70% yields. The dithio analog **5** was obtained similarly from the corresponding dithiooxamide in 61% yield. The molecular formulae of the complexes were established unambiguously by elemental analysis, mass spectrometry and X-ray crystallography.

High field multinuclear NMR spectra on the complexes reveal a very complicated set of peaks which point to a mixture of four isomers of each complex present in non-equivalent amounts. Mixtures of two isomers were found in the NMR data for **1**, **2a** and **2b** elsewhere[28,29] and were assigned as the diastereomers of the *anti* configuration with the same (ΔΔ or ΛΛ) configurations of the two octahedral Ir centres, and the *meso* (ΔΛ) form. The peaks corresponding to the extra two isomers observed in the NMR spectra of complexes **3a–d** here are thus from two diastereoisomers (ΔΔ/ΛΛ and ΔΛ) of the previously unknown *syn* configuration of oxamidato bridges in diiridium complexes and these observations are consistent with the X-ray crystal structures below. Representative NMR spectra are shown in the Supporting Information. Their detailed analysis and assignments would be very challenging and are beyond the scope of this article.

X-ray crystallography

All single crystals determined by X-ray crystallography were grown from mixtures of isomers in solution and the eleven crystal structures for **3a–5** are summarized in Table 1 with isomers identified as *anti* or *syn* at the (dithi)oxamidato bridge, where possible, and the diastereoisomer determined as the racemic (*rac*) ΔΔ/ΛΛ or *meso* ΔΛ form. Each Ir atom has a distorted octahedral coordination, the two cyclometalating 2-methyl-6-phenylpyridyl ligands (NC) having their N atoms *trans* to one another, and their C atoms *trans* to the bridging ligand.

For complex **3a**, the unsubstituted oxamidato bridge in both (isomorphous) solvates is disordered as observed for the previously reported unsubstituted oxamidato bridge analogs **1**[28] and **2a**.[29] The N and O atoms share symmetrically related positions, thus the *syn* or *anti*-configuration of the bridge cannot be established unequivocally from crystallographic data alone (Figure 2).

In the case of *N,N*-disubstituted oxamidato bridges, **3b** is remarkably the first example where both *anti* and *syn* isomers have been isolated and characterized crystallographically (Figures 3 and S1). The *anti*-configuration was established in the crystal structures for **3c** and **3d** (Figures S2 and S3) whereas the *syn*-configuration was present in **4** (Figures 4, S4 and S5).

In the structure of **5**·2CH_2Cl_2, the disorder of the dithioxamidato bridge (and its C_i symmetry) creates the same ambiguity as in **3a**, even though in **5**·2CH_2Cl_2 the individual positions of N and S atoms could be resolved, due to differences in atomic sizes (Figure 5). In the non-solvated **5**, the bridge is also disordered but in a peculiar way which allows to break this uncertainty (Figure S6). The observed occupancies of the bridge atoms can be rationalized as a superposition of two *syn*-configurations of opposite sense and one *anti*-configuration of the bridge, contributing 50%, 8% and 42%, respectively (Figure 6). Therefore, it can be concluded that cyclometalating

Table 1. Selected geometrical parameters of all diiridium complexes shown in Figure 1 from X-ray crystallography.

Compound	Bridge	Diastereomer	Molecular symmetry	Ir…Ir [Å]	C(Me)…C(Me) [Å]	C(Me)…bridge [Å]
1·2H_2O[28]	?	*meso*	-1	5.718		
2a·hexane[29]	?	*rac*	1	5.688		
2b·pentane·PhCl[29]	*anti*	*meso*	-1	5.726		
2c·pentane·PhCl[30]	*anti*	*meso*	-1	5.723		
3a·THF	?	*rac*	222	5.711	3.81	3.01 (N/O)
3a·CH_2Cl_2	?	*rac*	222	5.709	3.81	3.00 (N/O)
3b·2.75THF·0.5 MeOH	*anti*	*meso*	-1	5.804	3.58, 3.73	3.18, 3.21 (N), 2.95, 2.99 (O), 3.61, 3.70 (C)
3b·2.5PhCl	*syn*	*meso*	1	5.834	3.53, 3.82, 3.84, 3.85	3.14, 3.20 (N), 3.02, 3.15 (O)
3c·2CH_2Cl_2	*anti*	*rac*	1	5.773	3.63, 3.88	3.08, 3.17 (N), 2.93, 3.00 (O), 3.45, 3.48 (C)
3d·4CH_2Cl_2	*anti*	*meso*	−1	5.771	3.76	3.14 (N), 3.00 (O), 3.62 (C)
3d·THF	*anti*	*meso*	−1	5.794	3.71	3.17 (N), 3.01 (O), 3.63 (C)
4·PhCl	*syn*	*meso*	1	5.783	3.60, 4.08	3.14, 3.14 (N), 2.94, 2.99 (O)
4	*syn*	*meso*	1	5.806	3.67, 3.69, 3.75, 3.77	3.09, 3.11, 3.15, 3.22 (N), 2.92, 2.96, 2.98, 3.03 (O)
5·2CH_2Cl_2	?	*meso*	−1	6.116	4.17	3.04 (N), 3.14 (S)
5	*syn/anti*	*rac*	1	6.171	3.80, 3.99	3.00, 3.03 (N), 3.23, 3.33 (S)

Research Article
doi.org/10.1002/ejic.202300423

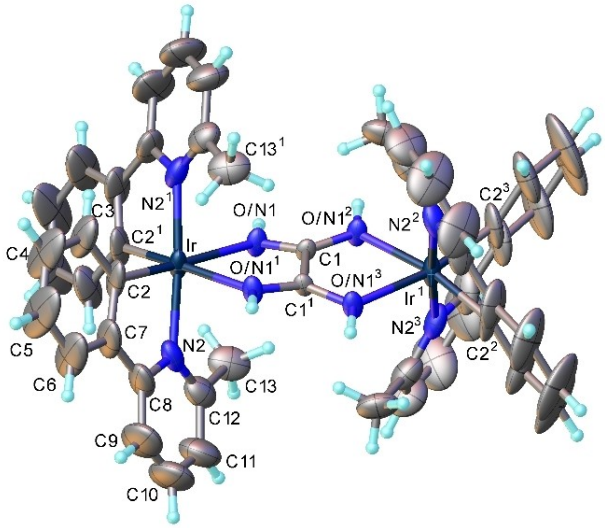

Figure 2. Molecule *rac*-**3a** in the crystal of **3a**·THF. Henceforth atomic displacement ellipsoids are drawn at 50% probability level. Symmetry transformations: (1) 5/4 – *x*, *y*, 5/4 – *z*; (2) 5/4 – *x*, 1/4 – *y*, *z*; (3) *x*, 1/4 – *y*, 5/4 – *z*.

2-methyl-6-phenylpyridyl ligands are perfectly compatible with both *syn* and *anti* configurations of the bridge, even with quite bulky substituents at the latter as shown in the distances between the methyl group and the bridging atoms (Table 1).

Molecule **3a** (Figure 2), in both **3a**·CH_2Cl_2 and **3a**·THF solvates studied, exists in the chiral form: the two Ir centres are related by a crystallographic twofold axis and have the same ($\Delta\Delta$ or $\Lambda\Lambda$) configuration, while the crystal is centrosymmetric and thus racemic. Complexes with *syn*-oxamidato bridges, **3b** and **4** (both in the **4**·PhCl and the non-solvated form), are *meso*, but with symmetrically independent Ir centres. Molecule **3c** is racemic, although the two Ir centres are not symmetrically related. Both **3d**·4CH_2Cl_2 and **3d**·THF solvates, have *meso* structures with the two metal centres related by a crystallographic inversion centre.

Most interestingly, the dithioxamidato-bridged complex **5** has been determined in both *rac* and *meso* forms (Figures 5 and 6). The **5**·2CH_2Cl_2 solvate is crystallographically centrosymmetric, i.e. *meso*, whereas the non-solvated crystal is racemic, with symmetrically unrelated Ir centres. Thus, methyl substituents at the cyclometalating ligands do not seem to discriminate between diastereoisomers. The only conceivable mechanism of such discrimination is intramolecular steric repulsion between methyl groups belonging to different Ir centres. It is noteworthy that in both *meso* and *rac* oxamidato-complexes, such contacts (Table 1) are considerably shorter than 4 Å, the double effective van der Waals radius of a methyl group.[34] Even though in *meso*-**5**, the longer thioxamidato bridge allows more leeway, a much shorter contact is realised in *rac*-**5**.

Electrochemistry

The redox properties of the diiridium complexes were studied by cyclic voltammetry (CV) and compared with those of the reported diiridium complexes **2a** and **2b** containing 4-mesityl-6-phenylpyridyl ligands (Table 2). All oxamidato-bridged complexes display two quasi-reversible, one-electron oxidation waves assigned to stepwise oxidation of the metal centred Ir^{3+}/Ir^{4+} redox couples. A comparison between the unsubstituted oxamidato-bridged complexes **2a** and **3a** reveals a 0.11 V difference in the first oxidation potential which is attributed to the electron-donating 2-methyl-6-phenylpyridyl cyclometalating

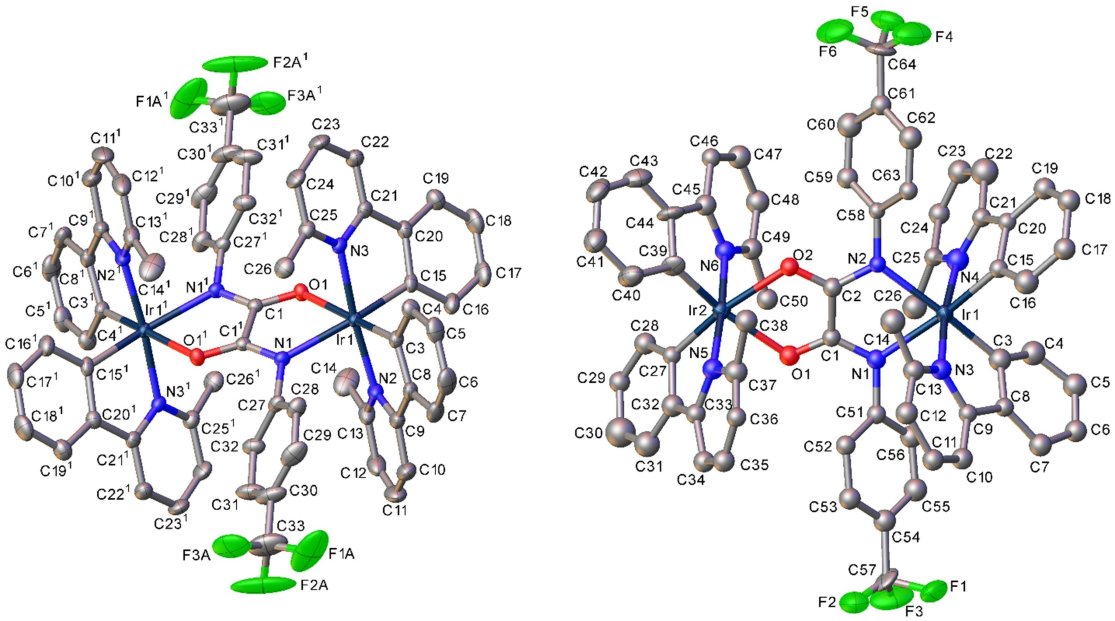

Figure 3. Molecular structures of *anti-rac*-**3b** (left) and *syn-meso*-**3b** (right) in **3b**·2.75THF·0.5 MeOH and **3b**·2.5PhCl respectively. H atoms are omitted for clarity.

Research Article
doi.org/10.1002/ejic.202300423

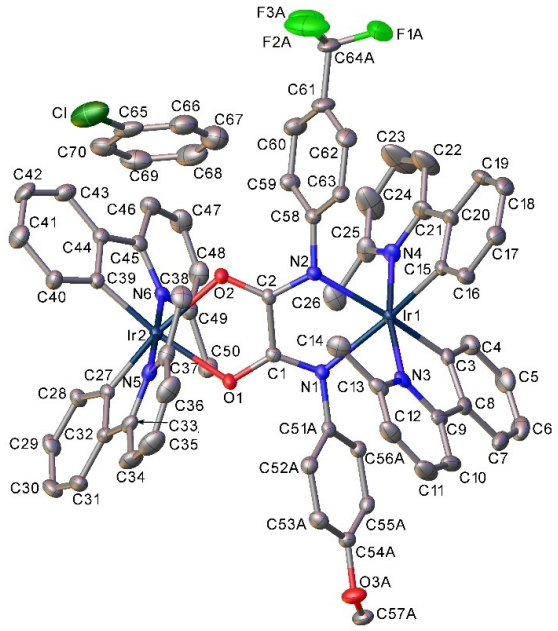

Figure 4. Molecular structure of *syn-meso*-**4**·PhCl. Minor positions of the disordered substituents and all H atoms are omitted for clarity.

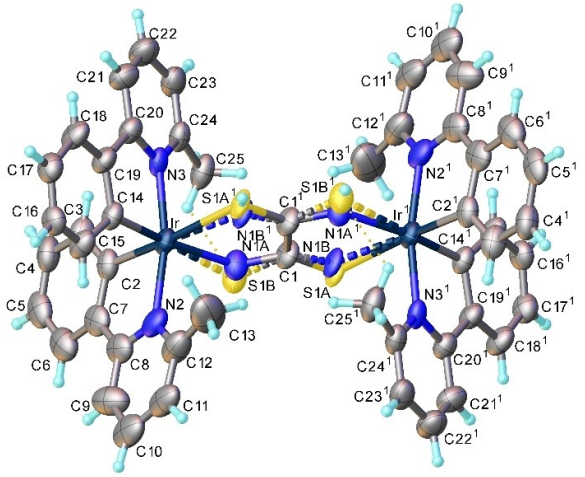

Figure 5. Molecule *meso*-**5** in the crystal of **5**·$2CH_2Cl_2$. Atoms generated by inversion centres, are primed. CH_2Cl_2 molecules are omitted for clarity.

ligand in **3a** with respect to the electron-withdrawing 4-mesityl-6-phenylpyridyl ligand. The 2-methyl-6-phenylpyridyl ligand also facilitates the stability of the monocationic species with a 210 mV difference between the first and second oxidation waves compared to 160 mV in **2a**.

For complexes with aryl-substituted bridges, **3b**–**4**, the increase in the first oxidation potentials corresponds to the increased electron-withdrawing properties of the substituents attached to the bridge with 0.26 V for **3c**, with the electron-donating methoxy groups, to 0.38 V for **3b**, containing electron-withdrawing trifluoromethyl groups (Figures 7 and S7). The methoxy groups also improve the stability of the monocationic species for **3c** and **4** with a 260–270 mV difference between the first and second oxidation waves.

The CV trace for the dithioxamido-bridged complex **5** showed a quasi reversible first oxidation wave and an irreversible second oxidation wave in contrast to the two quasi-reversible, one-electron oxidation waves observed for the oxamidato-bridged complexes. The dicationic species of **5** is unstable under these ambient conditions. The estimated difference of 300 mV between the two oxidation waves in **5** indicates that the dithioxamido bridge is stabilising the monocation species.

Photophysics

Absorption spectra for the oxamidato-bridged complexes **3a**–**4** reveal similar profiles with intense high energy peaks in the 250–300 nm region and low energy peaks in the 340–460 nm region with weaker intensities (Figure 8 and Table S1). These regions are assigned elsewhere for related iridium complexes as from ligand-centred transitions (LCT, $\pi\rightarrow\pi^*$) and mixed metal ligand to ligand charge transfers (MMLLCT) for 250–340 nm and 340–500 nm regions, respectively.[35] The dimethoxy derivative **3c** has a notable intense peak at 288 nm which is assumed to be specific to $\pi\rightarrow\pi^*$ LC transitions involving the methoxyphenyl groups. All oxamidato-bridged complexes **3a**–**4** have a virtually identical lowest energy absorption edge at 520 nm.

A different spectral profile to complexes **3a**–**4** is found for the dithioxamidato-bridged complex **5** where the peak intensities in the low energy MMLLCT region 350–550 nm are relatively strong compared to the high energy LC region. The lowest energy absorption band edge for **5** is at 590 nm implying that the dithioxamidato bridge contributes substantially to the lowest energy triplet states in **5**.

Emission data for complexes **3a**–**5** here, and the related oxamidato-bridged systems **1**, **2a** and **2b**,[24,25] are listed in Table 3 while emission spectra of **3a**–**5** are displayed in Figure 8. The unsubstituted oxamidato-bridged complex **3a** and the sulfur analog **5** show single broad emissions at 529 and 698 nm respectively. The small energy difference between the low energy absorption edge and the emission maximum in **3a** suggests that the lowest excited state geometry (T_1) for **3a** remains little changed in the excited and emission processes. By contrast, the substantial energy difference between the low energy absorption edge and the emission maximum in **5** at 590 and 698 nm, respectively, indicates that the lowest excited state geometry (T_1) alters considerably after excitation and before emission. The broad emissions observed from **3a** and **5** nevertheless are characteristic of a dominant triplet metal to ligand contribution rather than a ligand to ligand contribution where structured (vibronic) emission bands would be observed.[36]

The emission profiles for the aryl-substituted-oxamidato-bridged systems **3b**–**4** surprisingly are composed of two emission bands where one band is considerably more intense than the other. For the methoxy and fluoro derivatives **3c** and **3d**, the dominant emission band is at high energy (522–527 nm) like that found for **3a**. The dominant emission band for derivatives, **3b** and **4**, containing the strongly electron-with-

Research Article
doi.org/10.1002/ejic.202300423

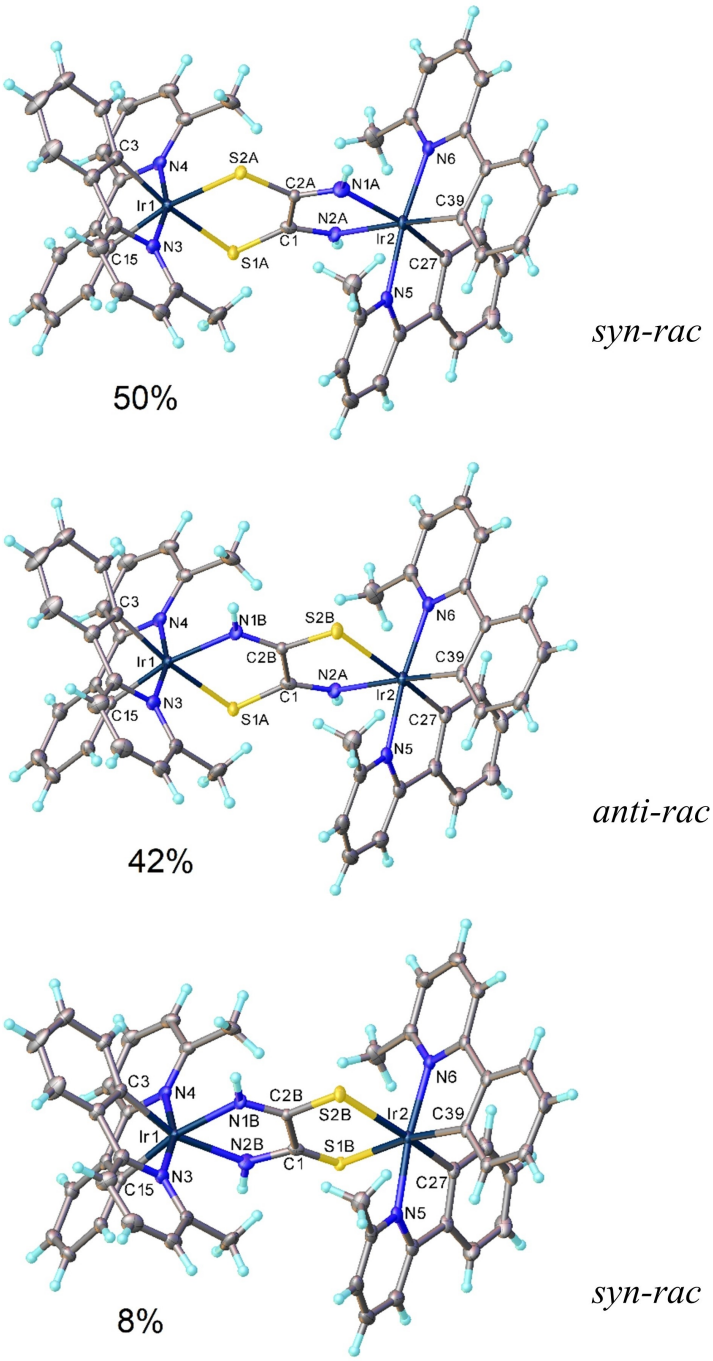

Figure 6. Interpretation of the disorder in non-solvated *rac*-**5** with superposition of two *syn* (of opposite sense) and one *anti*-configuration of the bridge.

drawing CF_3 groups is at low energy (689–701 nm) like the broad emission shown for **5**. These observations suggest two distinct excited states present in complexes **3b**–**4** are responsible for the dual emissions.

Compound **1** with 2-(4′-methylphenyl)pyridyl cyclometalating ligands (Figure 1) was reported to have a high photoluminescence quantum yield (PLQY) of 60% in dichloromethane (DCM).[28] Here, the presence of the methyl groups in the 2-methyl-6-phenylpyridyl cyclometalating ligands in the related unsubstituted oxamidato-bridged complex **3a** has a detrimental effect on the PLQY which is in the region of only 1% from deaerated DCM solutions. It is intriguing that the methyl group in a different position of the phenylpyridyl cyclometalating ligand has such a marked effect on the emission property in these diiridium complexes. The 2-methyl group in the complexes studied here facilitates a non-radiative pathway after excitation to the triplet excited state followed by structural rearrangement upon relaxation to the ground state. The much faster lifetimes observed for the complexes **3a**–**5** compared to the published[28,29] complexes **1**, **2a** and **2b**, are expected from

Research Article
doi.org/10.1002/ejic.202300423

Table 2. Cyclic voltammetry data of diiridium complexes **2**–**5** and comparison with experimental Ir…Ir distances and computed HOMO energies.

	$E_{1/2}^{Ox1}$ [V][a]	$E_{1/2}^{Ox2}$ [V][a]	$\Delta E_{1/2}$ [mV][a]	Ir….Ir [Å]	HOMO [eV][b]	HOMO [eV][c]
2a	+0.38	+0.54	160	5.688	−5.18	−5.25
2b	+0.40	+0.62	220	5.726	−5.20	−5.26
3a	+0.27	+0.48	210	5.709/5.711	−5.07	−5.09
3b	+0.38	+0.60	220	5.804/5.834	−5.18	−5.20
3c	+0.26	+0.52	260	5.773	−5.06	−5.11
3d	+0.31	+0.55	240	5.771/5.794	−5.11	−5.15
4	+0.29	+0.56	270	5.783/5.806	−5.09	−5.16
5	+0.26	[+0.56]	[300]	6.116/6.171	−5.06	−5.20

[a] 0.1 M ($^{n}Bu_4NPF_6$) in deaerated DCM solutions at 298 K, scan rate 100 mV s^{-1}, referenced to the internal decamethylferrocene/decamethylferrocenium couple (Fc*Me/Fc*Me$^+$) at −0.55 V with the ferrocenium/ferrocene (FcH/FcH$^+$) couple as reference at 0.00 V. [b] HOMO levels calculated from CV potentials by HOMO = −4.8 + ($-E_{1/2}^{ox}$), using ferrocene as the standard. [c] HOMO energies calculated from optimized geometries at B3LYP/LANL2DZ:3-21G*/IEF-PCM for *anti-rac* isomers for **3a**, **5** and *syn-meso* isomers for **3b**–**4**.

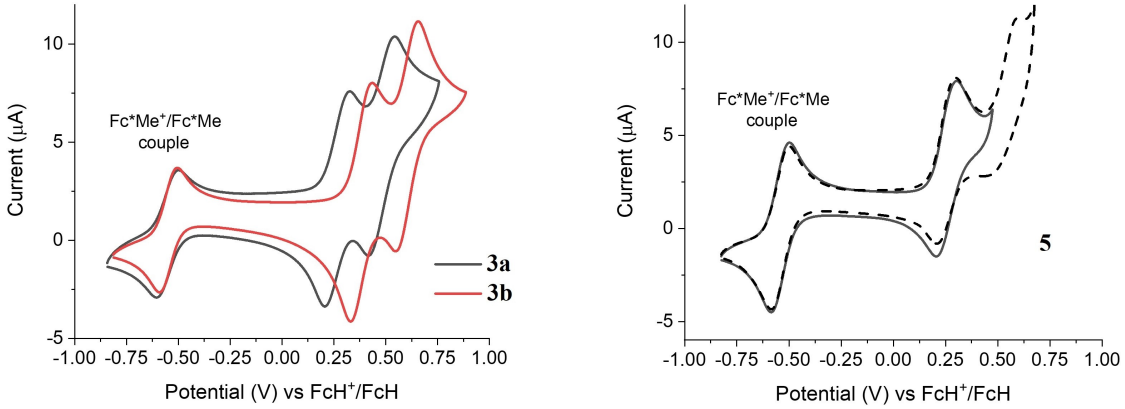

Figure 7. Cyclic voltammetry traces for **3a** and **3b** (left) and **5** (right). The dashed line in **5** shows that the second oxidation wave is irreversible.

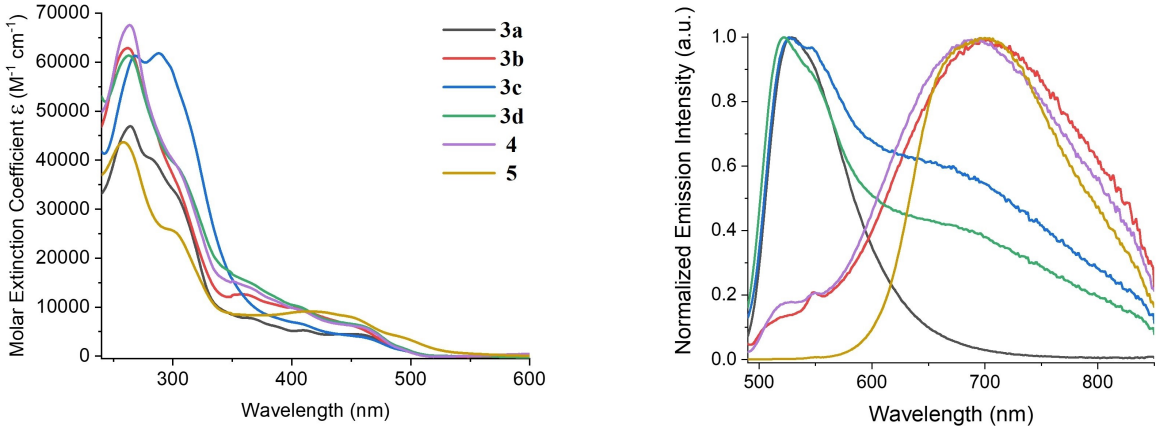

Figure 8. Absorption (left) and emission (right) spectra for diiridium complexes **3a**–**5**.

their low and high PLQY values, respectively.[18] The radiative rates k_r for **1** and the complexes **3a**–**5** are, however, similar in magnitude based on their PLQY and lifetime decay measurements.

Computations

Geometry optimizations were carried out on the four possible isomers of the diiridium complex in the 2-methyl-6-phenylpyridyl systems **3a**–**5** (Table S2). The total energy differences within these four diastereomers, *anti-rac, anti-meso*, *syn-rac* and

Research Article
doi.org/10.1002/ejic.202300423

Table 3. Emission data of diiridium complexes **1**–**5**.

	Emission maximum [nm]	PLQY [%]	Averaged lifetime τ_{av} [ns]	Radiative rate k_r[d] [s^{-1}]
1[a][28]	523	60	1600	3.75×10^5
2a[b][29]	529	73	840	8.69×10^5
2b[b][29]	522	63	1164	5.41×10^5
3a[a]	529	1[c]	75	1.33×10^5
3b[a]	701	1[c]	40	2.50×10^5
3c[a]	527	1[c]	31	3.23×10^5
3d[a]	522	1[c]	54	1.85×10^5
4[a]	689	1[c]	61	1.64×10^5
5[a]	698	1[c]	82	1.22×10^5

[a] Emission spectra and decay lifetimes obtained in degassed DCM solutions (10^{-5} M) with excitation wavelength of 470 nm at 20 °C and PLQYs were measured using an integrating sphere. [b] Emission spectra in degassed 2-methyl-tetrahydrofuran (MeTHF) solutions with excitation wavelength of 340 nm, PLQYs measured relative to $Ir(ppy)_3$ at $\Phi_{PL}=0.97$ in degassed MeTHF at 20 °C: estimated error ±5% and decay lifetimes were measured from poly(methyl methacrylate) (PMMA) thin films. The k_r values are estimated for **2a** and **2b** as PLQYs and lifetimes were recorded in different states. [c] High degree of error due to low intensity emission. [d] $k_r=\Phi_{PL}/\tau_{av}$.

syn-meso, in all complexes are insignificant with the largest energy difference of 2.1 kcal mol^{-1} between *anti rac* and *syn meso* in **5**. These values correspond with the mixtures of isomers observed in the syntheses of complexes **3a**–**5** and the conclusion is that the steric effect of the methyl group in the cyclometalating ligand on the isomer preference of the iridium product is remarkably negligible despite being close to the bridge and neighbouring methyl groups.

Electronic structure calculations reveal similar frontier molecular orbitals in the unsubstituted oxamidato-bridged *anti-rac*-**3a** as in the previously reported unsubstituted oxamidato-bridged *anti-rac*-**2a**: the HOMO is located on the iridium-phenyl moiety and the LUMO on the pyridyl groups (Figure 9 and Table S4). The dithioxamidato-bridged complex *anti-rac*-**5**, on the other hand, has considerable bridge contributions for both frontier orbitals (Figure 9 and Table S9).

The two aryl-substituted oxamidato-bridged systems *syn-meso*-**3c** and *syn-meso*-**3d** with methoxy and fluoro substituents, respectively, have similar frontier orbitals to *anti-rac*-**3a** (Tables S6 and S7) but with slightly increased bridge orbital contributions in the LUMOs. However, different frontier orbitals were present for the aryl-substituted oxamidato-bridged systems *syn-meso*-**3b** and *syn-meso*-**4** with significant bridge contributions to the LUMOs (Tables S5 and S8) at the expense of pyridyl group contributions, like in the LUMO for **5**. The calculated HOMO energies in all the complexes are in broad agreement with the experimental HOMO energies from the observed first oxidation potentials in the CV data (Table 2). The frontier orbital energies were shown to be little affected by different *syn* and *anti* configurations (Table S10).

There appears to be a correlation between the observed emission maxima and the bridge contribution in the LUMO in all complexes. Complexes **3a**, **3c** and **3d** with little bridge contributions in their frontier orbitals have high energy emission maxima at 522–527 nm, whereas complexes **3b**, **4** and **5** with dominant bridge contributions in the LUMOs have low energy emission maxima at 689–701 nm. These findings suggest the MMLCT excited states involving phenyl-iridium and pyridyl groups typically expected in emissions of cyclometalated 2-phenylpyridyl (ppy) iridium complexes,[35] are present in **3a**, **3c** and **3d**, whereas in **3b**, **4** and **5** there are different MMLCT excited states, where the bridging ligand contributes significantly. The apparent dual emissions from the aryl-substituted bridge complexes **3b**–**4** suggest that both distinct excited states are present in these complexes. The relative preference for one excited state over the other and thus the dominant emission observed depends on the CF_3, F or OMe substituents present in each complex. The possibility of dual emissions arising from different isomers in **3b** and **3c** based on their frontier orbitals is ruled out here as the LUMOs for the *anti-rac* isomers of **3b** and **3c** (Figures S8–S9 and Tables S11–S12) are similar to the LUMOs for the *syn-meso* isomers of **3b** and **3c**.

Conclusions

A diverse series of six diiridium complexes comprising 2-methyl-6-phenylpyridyl (2-Meppy) as the cyclometalating ligand and various oxamidato ligands or a μ_2-dithioxamidato ligand as the bridge has been synthesized as mixtures of diastereomers (*rac*, ΔΔ/ΛΛ and *meso*, ΔΛ) with bridges in *anti* and *syn* configurations. The remarkable variety of isomers present was confirmed by X-ray crystallography on single crystals grown from mixtures of each complex. The emission properties of these diiridium complexes are intriguing with two distinct excited states proposed from hybrid-DFT computations where broad high energy emissions arise from MLCT states involving the pyridyl groups of the cyclometalating ligand, and broad low energy emissions from MLCT states involving the bridge. In solution electrochemical experiments all the oxamidato-bridged complexes display two, quasi-reversible, one-electron oxidation

Research Article
doi.org/10.1002/ejic.202300423

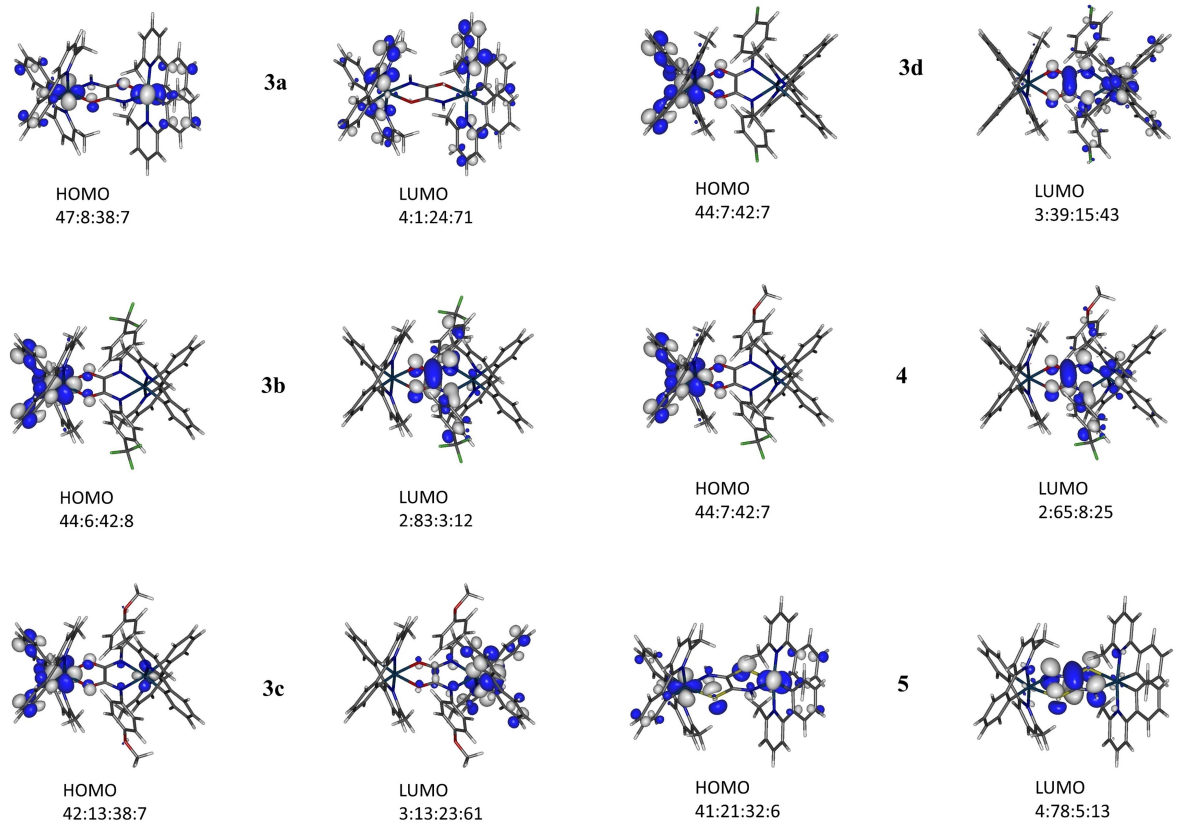

Figure 9. Frontier molecular orbitals for diiridium complexes as *anti-rac* isomers for **3 a**, **5** and *syn-meso* isomers for **3 b**–**4**. The Ir:bridge:phenyl:pyridyl ratios represent the atom/group MO contributions in percentages. Isocontours drawn at ± 0.04 e bohr$^{-3/2}$.

waves assigned to stepwise oxidation of the metal centred Ir^{3+}/Ir^{4+} redox couples with the difference between the first and second oxidation waves (210–270 mV) dependent on the bridge structure. In contrast, the dithioxamido-bridged complex showed a quasi reversible first oxidation wave and an irreversible second oxidation wave. Overall, this study provides new insights into structure-optoelectronic property relationships in diiridium complexes.

Experimental Section

General

All commercial chemicals were used without further purification unless otherwise stated. Solvents were dried through an HPLC column on an Innovative Technology Inc. solvent purification system. Column chromatography was carried out using 40–60 μm mesh silica. ^{1}H, ^{13}C{^{1}H}, 2D ^{1}H-^{1}H COSY and ^{1}H-^{13}C correlations (HSQC and HMBC) NMR spectra were recorded on a solution-state Varian V NMRS-600 spectrometer. Mass spectra were measured on a Waters Xevo Otof MS with an ASAP probe, a Thermoquest Trace or a Thermo-Finnigan DSQ. Elemental analyses were performed on a CE-400 Elemental Analyzer. The symmetrical oxalamide derivatives were prepared following the literature procedure from the appropriate aniline derivative and oxalyl chloride.[37]

The unsymmetrical oxalamide derivative ***N*^{1}-(4-methoxyphenyl)-*N*^{2}-[4-(trifluoromethyl)phenyl]oxalamide** used in the synthesis of complex **4** was prepared as follows. A mixture of 4-methoxyaniline (0.47 g, 3.82 mmol, 1 eq), triethylamine (1.07 ml, 7.6 mmol, 2 eq) and toluene (50 mL) were mixed under argon at 0 °C. Ethyl 2-oxo-2-{[4-(trifluoromethyl)phenyl]amino}acetate[38] (1.00 g, 3.82 mmol, 1 eq) was added and the mixture was stirred under reflux overnight. After cooling the solution to room temperature water (40 mL) was added to precipitate a solid, which was removed by filtration, washed with HCl (1 M, 40 mL) then water (40 mL), collected and shaken with hot ethanol (40 mL) to yield the oxalamide derivative as a white solid (1.1 g, 85 %). MS(ASAP) *m/z* 339.09 (M + H, 100 %). ^{1}H NMR (700 MHz, DMSO-d$_6$) δ 11.18 (s, 1H, N^{2}H), 10.81 (s, 1H, N^{1}H), 8.10 (d, $J_{HH} = 9.2$ Hz, 2H, aryl CH at N^{2}), 7.79 (d, $J_{HH} = 9.2$ Hz, 2H, aryl CH at N^{1}), 7.77 (d, $J_{HH} = 9.2$ Hz, 2H, aryl CH at N^{2}), 6.96 (d, $J_{HH} = 9.2$ Hz, 2H, aryl CH at N^{1}), 3.76 (s, $J_{HH} = 9.2$ Hz, 3H, OCH_3); ^{19}F{^{1}H} NMR (162 MHz, DMSO-d$_6$) δ −60.5 (s).

Tetrakis(2-methyl-6-phenylpyridine-*C*^{2},*N*′)-bis(μ-chloro)diiridium(III). Following the literature procedure[39] a mixture of 2-methyl-6-phenylpyridine (386 mg, 1.96 mmol, 2 eq), 2-ethoxyethanol/water (10/5 ml) and $IrCl_3.H_2O$ (0.294 g, 0.98 mmol, 1 eq) under argon was heated with stirring at 120 °C for 12 h. The solvent was removed under vacuum and the crude product was dissolved in DCM (100 mL) and the organic layer was separated and dried over $MgSO_4$, filtered and the DCM removed. The solid was washed with hexane to yield a product presumed to be the bis(μ-chloro)-bridged dimer (**D1**) (410 mg, 63 %) which was used without further purification. Degradation of the presumed dimer was rapid and no NMR or mass spectra corresponding to **D1** (or a related species that could be expected to react similarly to **D1**)[40] could be obtained. The presumed dimer was therefore used immediately in subsequent reactions without characterisation.

Research Article
doi.org/10.1002/ejic.202300423

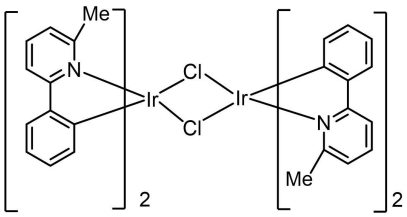

D1

Complex 3a. Solutions of sodium methoxide (62 mg, 1.12 mmol, 2.6 eq) in methanol (2 mL) and oxalamide (51.9 mg, 0.56 mmol, 1.3 eq) in methanol (10 mL) were mixed and stirred for 30 min at 20 °C in a round bottom flask. A solution of dichloro-dimer (**D1**) (500 mg, 0.44 mmol, 1 eq) in THF (45 mL) was added. The reaction mixture was stirred at 20 °C for 24 h. The solvent was removed and the crude product was dissolved in DCM (80 mL). Water (40 mL) was added and the DCM layer was separated and dried over magnesium sulfate then filtered. Methanol (30 mL) was added to the DCM. The solvent was partly removed using a rotavapor leaving the crude solid product and some solvent. The solid was filtered and purified by column chromatography over silica gel, eluting with DCM (saturated with K_2CO_3 and 2% Et_3N) to give complex **3a** (0.35 g, 69%) as a yellow-orange solid. MS(MALDI-ToF) m/z 1143.36 ([M^+, ^{191}Ir, ^{193}Ir], 100%). Anal. Calcd. For $C_{50}H_{42}Ir_2N_6O_2$: C, 52.50; H, 3.70; N, 7.35. Found: C, 52.22; H, 4.00; N, 7.25%. Crystallisation either from a mixture of CH_2Cl_2/hexane, or from a mixture of THF/hexane gave **3a**·CH_2Cl_2 and **3a**·THF, respectively.

Complex 3b. Solutions of sodium methoxide (22 mg, 0.407 mmol, 2.6 eq) in methanol (1 mL), *N,N'*-bis(trifluoromethylphenyl)oxalamide[41] (76 mg, 0.204 mmol, 1.3 eq) in methanol (10 mL) were mixed and stirred for 30 min at 20 °C in a round-bottom flask. Dichloro-dimer (**D1**) (175 mg, 0.155 mmol, 1 eq) in THF (30 mL) was added. The reaction mixture was stirred at 20 °C for 24 h. The solvent was removed and the crude product was dissolved in DCM (50 mL). Water (25 ml) was added and the DCM layer was separated and dried over magnesium sulfate then filtered. Hexane (20 mL) was added to the DCM. The solvent was partly removed using a rotavapor leaving the crude solid product and some solvent. The solid was filtered and purified by column chromatography over silica gel, eluting with DCM:hexane (1:1 v/v), then DCM : hexane (2:1 v/v) then DCM (saturated with K_2CO_3 and 2% Et_3N) to give complex **3b** (135 mg, 61%) as a yellow-orange solid. MS(MALDI-ToF) m/z 1432.1 ([M + H, ^{191}Ir, ^{193}Ir], 100%). Anal. Calcd. for $C_{64}H_{48}F_6Ir_2N_6O_2$: C, 53.70 ; H, 3.38; N, 5.87. Found: C, 53.41; H, 3.36; N, 5.56%. *Anti*-**3b** was crystallized from a THF/methanol mixture, *syn*-**3b** from chlorobenzene/pentane mixture.

Complex 3c. Following the procedure for complex **3b**, the following reagents were used: sodium methoxide (22 mg, 2.6 eq) in methanol (1 mL), *N,N'*-bis(4-methoxyphenyl)oxalamide[42] (61 mg, 1.3 eq) in methanol (10 mL) and dichloro-dimer (**D1**) (175 mg, 0.155 mmol, 1 eq) in 30 mL THF (30 mL). The crude product was purified by column chromatography over silica gel, eluting sequentially with DCM:hexane (2:1 v/v), DCM:hexane (5:1 v/v) then DCM (saturated with K_2CO_3 and 2% Et_3N) to give complex **3c** (130 mg, 62%). Crystallization from a CH_2Cl_2/hexane mixture gave crystals of **3c**·$2CH_2Cl_2$. MS(MALDI-ToF) m/z 1356.1 ([M + H, ^{191}Ir, ^{193}Ir], 100%). Anal. Calcd. for $C_{64}H_{54}Ir_2N_6O_4 \cdot 2CH_2Cl_2$: C, 51.97; H, 3.83; N, 5.51. Found: C, 51.66; H, 4.00; N, 5.20%.

Complex 3d. Following the procedure for complex **3b**, the following reagents were used: sodium methoxide (61 mg, 2.6 eq), *N,N'*-bis(4-fluorophenyl)oxalamide[43] (158 mg, 1.3 eq) in methanol (10 mL) and dichloro-dimer (500 mg, 0.44 mmol, 1 eq) in THF (45 mL) was added. The reaction mixture was stirred at r.t for 24 h. The solvent was removed and the crude product was dissolved in DCM (100 mL). Water (50 mL) was added and the DCM layer was dried over magnesium sulfate then filtration. Hexane (20 mL) was added to the DCM. The solvent was partially removed under vacuum, leaving a solid product and some solvent. The product was isolated by filtration and purified by column chromatography over silica gel, eluting with Et_2O (saturated with K_2CO_3 and containing 2% Et_3N) then with DCM (saturated with K_2CO_3 containing 2% Et_3N) to give complex **3d** (380 mg, 64%). Crystallization either from a mixture of CH_2Cl_2/hexane, or from a mixture of THF/hexane, gave crystals of **3d**·$4CH_2Cl_2$ and **3d**·THF, respectively. MS(MALDI-ToF) m/z 1330.2 ([M + H, ^{191}Ir, ^{191}Ir], 100%). Anal. Calcd. for $C_{62}H_{48}F_2Ir_2N_6O_2 \cdot 4CH_2Cl_2$: C, 47.43; H, 3.38; N, 5.03. Found: C, 47.80; H, 3.71; N, 4.77%.

Complex 4. Following the procedure for complex **3b**, the following reagents were used: sodium methoxide (71 mg, 3 eq) in methanol (2 mL), N^1-(4-methoxyphenyl)-N^2-[4-(trifluoromethyl)phenyl]-oxalamide (0.224 g, 1.5 eq) in methanol (6 mL) and dichloro-dimer **D1** (500 mg, 0.44 mmol, 1 eq) in THF (20 mL) was added. After the reaction was complete, as described for **3b**, methanol (30 mL) was added to the DCM. Column chromatography over silica gel, eluting with DCM (saturated with K_2CO_3 and 2% Et_3N) gave complex **4** (0.40 g, 73%). Crystallization of **4** from chlorobenzene/pentane mixture initially yielded needle-like crystals of unsolvated **4a**, which later spontaneously recrystallized into plate-like crystals of **4**·PhCl. MS(MALDI-ToF) m/z 1394.3 ([M + H, ^{191}Ir, ^{193}Ir], 100%). Anal. Calcd. for $C_{64}H_{51}F_3Ir_2N_6O_3$: C, 55.16; H, 3.69; N, 6.03. Found: C, 55.40; H, 3.66; N, 6.21%.

Complex 5. Following the procedure for complex **3a** the following reagents were used: sodium methoxide (61 mg, 2.6 eq) in methanol (2 mL), dithioxalamide (70 mg, 1.3 eq) in methanol (10 mL) and dichloro-dimer **D1** (500 mg, 0.44 mmol, 1 eq) in THF (45 mL) was added. After the reaction was complete, as described for **3b**, methanol (30 mL) was added to the DCM. Column chromatography over silica gel, elution with DCM (saturated with K_2CO_3 and 2% Et_3N) gave complex **5** (310 mg, 60%). Crystallization of **5** from CH_2Cl_2/hexane yielded **5**·$2CH_2Cl_2$; crystallization from chlorobenzene/pentane yielded non-solvated crystals of **5**. MS(MALDI-ToF) m/z 1174.2 ([M + H, ^{191}Ir, ^{191}Ir], 100%). Anal. Calcd. For $C_{50}H_{42}F_3Ir_2N_6S_2$: C, 51.09; H, 3.60; N, 7.15. Found: C, 50.77; H, 3.66; N, 7.44%.

X-Ray structure determination

In general, all the isomers that were obtained after extensive crystallisation experiments were separated and analysed. In each crystallisation, the crystals were fairly uniform in habit, and more than one crystal was checked for unit cell parameters. Typically, only one crystal form was obtained. Also, the same isomer was seen growing from different solvents. Of course, when the crystal is a solid solution of different isomers (as **5**), it is perfectly possible that different crystals have a different ratio of components. For most samples, X-ray diffraction experiments were carried out on a Bruker D8 Venture 3-circle diffractometer, equipped with PHOTON 100 CMOS area detector, using $Mo_{K\alpha}$ ($Cu_{K\alpha}$ for *syn*-**3b**·2.5PhCl) radiation from Incoatec IμS microsources with focusing mirrors. The crystals were cooled using Cryostream 700 open-flow N_2 gas cryostat (Oxford Cryosystems). The data were collected in shutterless mode by narrow frame ω scans covering full sphere of reciprocal space, using APEX3 v.2016.1-0 software, reflection intensities integrated using SAINT v8.38 A software (Bruker AXS, 2016), and corrected for absorption by numerical integration based on crystal face-indexing, using SADABS software[44] or TWINABS (for **3d**·THF).

For **3d**·$4CH_2Cl_2$ and **5**·$2CH_2Cl_2$, the experiments were performed at Beamline I19 (EH1) of Diamond Light Source (RAL) on a dual air-bearing fixed-χ diffractometer with pixel-array photon-counting Dectris Pilatus 2 M detector,[45] using undulator radiation monochromated with double-crystal Si(111) (λ = 0.6889 Å). The crystal was cryo-mounted using remote-controlled BART robot[46] and cooled to 100 K using a Cryostream cryostat. Full sphere of reciprocal space was nominally covered by one run of 900 thin-slice φ-scans and 3 runs of 850 thin-slice ω-scans each (scan width 0.2°, 0.2 s exposure). Substantial radiation decay was observed for **3d**·$4CH_2Cl_2$. The computations were carried out using Diamond I19 EH1 GDA[45] and DIALS software.[47] The diffraction images were merged pairwise and converted to Bruker format using cbf_to_sfrm.py program[48] and further processed with APEX3 and SAINT software. Structures **3c**, **3d**·$4CH_2Cl_2$, **5**·$2CH_2Cl_2$ and **5** were solved by dual-space intrinsic phasing, using SHELXT 2018/2 program,[49] other structures by direct methods, using SHELXS 2013/1 program.[50] All structures were refined by full-matrix least squares using SHELXL software[51] on Olex2 platform.[52] Methyl groups were refined as rigid (rotating) bodies, other H atoms in riding model. Deposition Numbers 2278703 (for *rac*-**3a**-dcm), 2278715 (for *rac*-**3a**-thf), 2278742 (for *anti*-**3b**), 2278750 (for *anti-rac*-**3c**), 2278780 (for *anti*-**3d**-dcm), 2278781 (for *anti*-**3d**-thf), 2278804 (for **4**·PhCl), 2278817 (for *syn-meso*-**4**), 2278820 (for *meso*-**5**-dcm), 2278821 (for *rac*-**5**) and 2278738 (for *syn*-**3b**) contain the supplementary crystallographic data for this paper. These data are provided free of charge by the joint Cambridge Crystallographic Data Centre and Fachinformationszentrum Karlsruhe Access Structures service.

Electrochemistry

Cyclic voltammograms were recorded at a scan rate of 100 $mV\,s^{-1}$ at room temperature using an air-tight single-compartment three-electrode cell equipped with a Pt disk working electrode, Pt wire counter electrode, and Pt wire pseudo-reference electrode. The cell was connected to a computer-controlled Autolab PG-STAT 30 potentiostat. The solutions contained the complex and *n*-Bu_4NPF_6 (0.1 M) as the supporting electrolyte in dichloromethane (DCM). All potentials were determined with the decamethylferrocene/decamethylferrocenium couple as an internal reference in DCM at −0.55 V for the usual reference standard of the ferrocene/ferrocenium couple (FcH/FcH^+) in DCM at 0.0 V.

Photophysical measurements

Solution-state measurements were carried out in quartz cuvettes with a path length of 1 cm. Absorbance spectra were measured on a Cary 5000 UV-Vis-NIR spectrometer with Cary WinUV Scan software. Emission spectra were recorded on a Jobin Yvon Fluorolog-3 luminescence spectrometer with a CCD detector using FluorEssence software. Photoluminescence quantum yields (PLQYs) were obtained using a calibrated Quanta-φ integrating sphere coupled with a Jobin Yvon FluoroLog-3 spectrometer and PMT detector (0.5 s integration time) and analysed using FluorEssence software. Time-resolved measurements (TCSPC, time-correlated single-photon counting) were performed on a Horiba Deltaflex system with EzTime software.

Computations

All calculations were carried out with the Gaussian 16 package.[53] The 24 optimized geometries of the four isomers of **3a**–**5** were carried out using B3LYP[54] with the pseudopotential (LANL2DZ)[55] for iridium and 3–21G* basis set[56] for all other atoms. This model chemistry was selected on the basis of good agreements between experimental and computed data in related diiridium complexes elsewhere.[17,18,29] The IEF-PCM solvation model[57] was applied using methanol as solvent throughout based on the reaction solvent used in the diiridium complexes, **3a**–**5**. All geometries were found to be true minima with no imaginary frequencies found. Electronic structure calculations at B3LYP/LANL2DZ:3-21G*/IEF-PCM were used to generate MO figures and orbital contributions for **3a**–**5** with the aid of Gabedit[58] and GaussSum[59] packages, respectively.

Acknowledgements

The Diamond Light Source is thanked for the award of instrument time on Station I19 (CY-22240) and the instrument scientists for their kind support. Funding for this research was provided by Deanship of Scientific Research at Prince Sattam Bin Abdulaziz University (grant No. 19803/01/2022 to A. M'hamedi).

Conflict of Interests

The authors declare no conflict of interest.

Data Availability Statement

The data that support the findings of this study are available in the supplementary material of this article.

Keywords: iridium · bimetallic · luminescence · X-ray crystallography · density functional theory

[1] *Iridium(III) in Optoelectronic and Photonics Applications* (Ed.: E. Zysman-Colman), Wiley, **2017**.
[2] T.-Y. Li, J. Wu, Z.-G. Wu, Y.-X. Zheng, J.-L. Zuo, Y. Pan, *Coord. Chem. Rev.* **2018**, *374*, 55–92.
[3] L. He, C. Tan, Q. Cao, Z. Mao, *Prog. Chem.* **2018**, *30*, 1548–1556.
[4] Z. Q. Chen, Z. Q. Bian, C. H. Huang, *Adv. Mater.* **2010**, *22*, 1534–1539.
[5] T. You, W. Nam, *Chem. Soc. Rev.* **2012**, *41*, 7061–7084.
[6] L. Xiao, Z. Chen, B. Qu, J. Luo, S. Kong, Q. Gong, J. Kido, *Adv. Mater.* **2011**, *23*, 926–952.
[7] K. M. Kuznetsov, I. S. Kritchenkov, J. R. Shakirova, V. V. Gurzhiy, V. V. Pavlovskiy, V. V. Porsev, V. V. Sokolov, S. P. Tunik, *Eur. J. Inorg. Chem.* **2021**, 2163–2170.
[8] C. E. Elgar, H. Y. Otaif, J. M. Beames, P. N. Horton, S. J. Coles, A. J. Hallett, S. P. O'Kell, S. J. A. Pope, *Eur. J. Inorg. Chem.* **2023**, e202300102.
[9] G. Millan, M. Nieddu, I. P. Lopez, C. Ezquerro, J. R. Berenguer, I. M. Larrayoz, J. G. Pichel, E. Lalinde, *Dalton Trans.* **2023**, *52*, 6360–6374.
[10] S. Paziresh, R. B. Aghakhanpour, H. R. Shahsavari, V. Dolatyari, I. Ara, S. M. Nabavizadeh, *New J. Chem.* **2023**, *47*, 1378–1387.
[11] S. Sprouse, K. A. King, P. J. Spellane, R. J. Watts, *J. Am. Chem. Soc.* **1984**, *106*, 6647–6653.
[12] G. Li, D. G. Congrave, D. Zhu, Z. Su, M. R. Bryce, *Polyhedron* **2018**, *140*, 146–157.
[13] G. Li, D. Zhu, X. Wang, Z. Su, M. R. Bryce, *Chem. Soc. Rev.* **2020**, *49*, 765–838.
[14] R. E. Daniels, S. Culham, M. Hunter, M. C. Durrant, M. R. Probert, W. Clegg, J. A. G. Williams, V. N. Kozhevnikov, *Dalton Trans.* **2016**, *45*, 6949–6962.
[15] X. Yang, X. Xu, J. S. Dang, G. Zhou, C. L. Ho, W. Y. Wong, *Inorg. Chem.* **2016**, *55*, 1720–1727.
[16] X. Yang, X. Chen, J. Dang, Y. Sun, Z. Feng, Z. Tian, G. Zhou, Z. Wu, *Chem. Eng. J.* **2020**, *391*, 123505.

[17] Y. Zheng, A. S. Batsanov, M. A. Fox, H. A. Al-Attar, K. Abdullah, V. Jankus, M. R. Bryce, A. P. Monkman, *Angew. Chem. Int. Ed.* **2014**, *53*, 11616–11619.
[18] D. G. Congrave, Y.-T. Hsu, A. S. Batsanov, A. Beeby, M. R. Bryce, *Dalton Trans.* **2018**, *47*, 2086–2098.
[19] J. L. Liao, P. Rajakannu, P. Gnanasekaran, S. R. Tsai, C. H. Lin, S. H. Liu, C. H. Chang, G. H. Lee, P. T. Chou, Z. N. Chen, Y. Chi, *Adv. Opt. Mater.* **2018**, *6*, 1800083.
[20] Y. Yuan, P. Gnanasekaran, Yu-W. Chen, G-H. Lee, S-F. Ni, C-S. Lee, Y. Chi, *Inorg. Chem.* **2020**, *59*, 523–532.
[21] X.-H. Yang, M. Li, H. Peng, Q. Zhang, S.-X. Wu, W.-Q. Xiao, X.-L. Chen, Z.-G. Niu, G.-Y. Chen, G.-N. Li, *Eur. J. Inorg. Chem.* **2019**, 847–855.
[22] G. Li, X. Ren, G. Shan, W. Che, D. Zhu, L. Yan, Z. Su, M. R. Bryce, *Chem. Commun.* **2015**, *51*, 13036–13039.
[23] Y. Jiang, G. Li, W. Che, Y. Liu, B. Xu, G. Shan, D. Zhu, Z. Su, M. R. Bryce, *Chem. Commun.* **2017**, *53*, 3022–3025.
[24] Y. He, G. Fu, W. Li, B. Wang, T. Miao, M. Tan, W. Feng, X. Lü, *J. Lumin.* **2020**, *218*, 116847.
[25] M–G. La-Placa, A. M. Igual-Muñoz, J. Romero, R. E. Daniels, V. N. Kozhevnikov, M. Sessolo, H. J. Bolink, *ECS J. Solid State Sci. Technol.* **2019**, *8*, R84–R87.
[26] K. Sasakura, K. Okamoto, K. Ohe, *Eur. J. Inorg. Chem.* **2020**, 1894–1901.
[27] J. Fernández-Cestau, N. Giménez, E. Lalinde, P. Montaño, M. T. Moreno, S. Sánchez, *Organometallics* **2015**, *34*, 1766–1778.
[28] M. Graf, R. Czerwieniec, K. Sünkel, *Z. Anorg. Allg. Chem.* **2013**, *639*, 1090–1094.
[29] A. M'hamedi, M. A. Fox, A. S. Batsanov, H. A. Al-Attar, A. P. Monkman, M. R. Bryce, *J. Mater. Chem. C* **2017**, *5*, 6777–6789.
[30] A. M'hamedi, A. S. Batsanov, *Acta Crystallogr. Sect. E* **2020**, *76*, 392–399.
[31] I. Haiduc, *J. Coord. Chem.* **2020**, *73*, 1619–1700.
[32] S. Lanza, G. Bruno, F. Nicolò, A. Rotondo, G. Tresoldi, *Eur. J. Inorg. Chem.* **2002**, 65–72.
[33] B. Askari, H. A. Rudbari, N. Micale, T. Schirmeister, T. Efferth, E.-J. Seo, G. Bruno, K. Schwickert, *Dalton Trans.* **2019**, *48*, 15869–15887.
[34] L. Pauling, The Nature of the Chemical Bond and the Structure of Molecules and Crystals; an Introduction to Modern Structural Chemistry (3rd ed.). Ithaca (NY): Cornell University Press. 1960, pp. 543–562. ISBN 0–8014-0333-2.
[35] a) S. Lamansky, P. Djurovich, D. Murphy, F. Abdul-Razzaq, H.-E. Lee, C. Adachi, P. E. Burrows, S. R. Forrest, M. E. Thompson, *J. Am. Chem. Soc.* **2001**, *123*, 4304–4312; b) P. J. Hay, *J. Phys. Chem. A* **2002**, *106*, 1634–1641.
[36] A. Tsuboyama, H. Iwawaki, M. Furugori, T. Mukaide, J. Kamatani, S. Igawa, T. Moriyama, S. Miura, T. Takiguchi, S. Okada, M. Hoshino, K. Ueno, *J. Am. Chem. Soc.* **2003**, *125*, 12971–12979.
[37] I. Welterlich, O. Charov, B. Tieke, *Macromolecules* **2012**, *45*, 4511–4519.
[38] F. Pape, J. F. Teichert, *Synthesis* **2017**, *49*, 2470–2482.
[39] M. Nonoyama, *Bull. Chem. Soc. Jpn.* **1974**, *47*, 767–768.
[40] C. Xu, Z.-Q. Wang, X.-M. Dong, X.-Q. Hao, X.-M. Zhao, B.-M. Ji, M.-P. Song, *Inorg. Chim. Acta* **2011**, *373*, 306–310.
[41] M. R. Crawley, D. Zhang, A. N. Oldacre, C. M. Beavers, A. E. Friedman, T. R. Cook, *J. Am. Chem. Soc.* **2021**, *143*, 1098–1106.
[42] J. Wang, H. Hou, Y. Hu, J. Lin, M. Wu, Z. Zheng, X. Xu, *Tetrahedron Lett.* **2021**, *65*, 152801.
[43] D. Taher, F. F. Awwadi, M. Al-Noaimi, L. K. Khader, H. K. Juwhari, H. Amarne, M. H. Kailani, A. Ibdah, *Inorg. Chim. Acta* **2019**, *487*, 409–418.
[44] L. Krause, R. Herbst-Irmer, G. M. Sheldrick, D. Stalke, *J. Appl. Crystallogr.* **2015**, *48*, 3–10.
[45] D. R. Allan, H. Nowell, S. A. Barnett, M. R. Warren, A. Wilcox, J. Christensen, L. K. Saunders, A. Peach, M. T. Hooper, L. Zaja, S. Patel, L. Cahill, R. Marshall, S. Trimnell, A. J. Foster, T. Bates, S. Lay, M. A. Williams, P. V. Hathaway, G. Winter, M. Gerstel, R. W. Wooley, *Crystals* **2017**, *7*, 336.
[46] N. T. Johnson, P. G. Waddell, W. Clegg, M. R. Probert, *Crystals* **2017**, *7*, 360.
[47] G. Winter, D. G. Waterman, J. M. Parkhurst, A. S. Brewster, R. J. Gildea, M. Gerstel, L. Fuentes-Montero, M. Vollmar, T. Michels-Clark, I. D. Young, N. K. Sauter, G. Evans, *Acta Crystallogr. Sect. D* **2018**, *74*, 85–97.
[48] N. T. Johnson, M. R. Probert, *cbf to sfrm – 2016 (alpha version)*, Newcastle University, UK. https://github.com/nu-xtal-tools/cbf to sfrm/blob/master/cbf to sfrm 2016.py Accessed 11/08/2022.
[49] G. M. Sheldrick, *Acta Crystallogr. Sect. A* **2015**, *71*, 3–8.
[50] G. M. Sheldrick, *Acta Crystallogr. Sect. A* **2008**, *64*, 112–122.
[51] G. M. Sheldrick, *Acta Crystallogr. Sect. C* **2015**, *71*, 3–8.
[52] O. V. Dolomanov, L. J. Bourhis, R. J. Gildea, J. A. K. Howard, H. Puschmann, *J. Appl. Crystallogr.* **2009**, *42*, 339–341.
[53] Gaussian 16, Revision B.01, M. J. Frisch, G. W. Trucks, H. B. Schlegel, G. E. Scuseria, M. A. Robb, J. R. Cheeseman, G. Scalmani, V. Barone, G. A. Petersson, H. Nakatsuji, X. Li, M. Caricato, A. V. Marenich, J. Bloino, B. G. Janesko, R. Gomperts, B. Mennucci, H. P. Hratchian, J. V. Ortiz, A. F. Izmaylov, J. L. Sonnenberg, D. Williams-Young, F. Ding, F. Lipparini, F. Egidi, J. Goings, B. Peng, A. Petrone, T. Henderson, D. Ranasinghe, V. G. Zakrzewski, J. Gao, N. Rega, G. Zheng, W. Liang, M. Hada, M. Ehara, K. Toyota, R. Fukuda, J. Hasegawa, M. Ishida, T. Nakajima, Y. Honda, O. Kitao, H. Nakai, T. Vreven, K. Throssell, J. A. Montgomery, Jr., J. E. Peralta, F. Ogliaro, M. J. Bearpark, J. J. Heyd, E. N. Brothers, K. N. Kudin, V. N. Staroverov, T. A. Keith, R. Kobayashi, J. Normand, K. Raghavachari, A. P. Rendell, J. C. Burant, S. S. Iyengar, J. Tomasi, M. Cossi, J. M. Millam, M. Klene, C. Adamo, R. Cammi, J. W. Ochterski, R. L. Martin, K. Morokuma, O. Farkas, J. B. Foresman, D. J. Fox, Gaussian, Inc., Wallingford CT, **2016**.
[54] a) A. D. Becke, *J. Chem. Phys.* **1993**, *98*, 5648–5652; b) C. Lee, W. Yang, R. G. Parr, *Phys. Rev. B* **1988**, *37*, 785–789.
[55] a) T. H. Dunning Jr., P. J. Hay in *Modern Theoretical Chemistry*, *Vol. 3* (Ed.: H. F. Schaefer III), Plenum, New York, **1976**; b) P. J. Hay, W. R. Wadt, *J. Chem. Phys.* **1985**, *82*, 270–283; c) W. R. Wadt, P. J. Hay, *J. Chem. Phys.* **1985**, *82*, 284–298; d) P. J. Hay, W. R. Wadt, *J. Chem. Phys.* **1985**, *82*, 299–310.
[56] a) G. A. Petersson, M. A. Al-Laham, *J. Chem. Phys.* **1991**, *94*, 6081–6090; b) G. A. Petersson, A. Bennett, T. G. Tensfeldt, M. A. Al-Laham, W. A. Shirley, J. Mantzaris, *J. Chem. Phys.* **1988**, *89*, 2193–2218.
[57] J. Tomasi, B. Mennucci, E. Cancès, *J. Mol. Struct.* **1999**, *464*, 211–226.
[58] A. R. Allouche, *J. Comput. Chem.* **2011**, *32*, 174–182.
[59] N. M. O'Boyle, A. L. Tenderholt, K. M. Langner, *J. Comput. Chem.* **2008**, *29*, 839–845.

Manuscript received: July 4, 2023
Revised manuscript received: September 1, 2023
Accepted manuscript online: September 15, 2023
Version of record online: October 4, 2023